Revealing the stoichiometric tolerance of lead tri-halide perovskite thin-films

Alexandra J. Ramadan,[*†] Maryline Ralaiarisoa,[¥] Fengshuo Zu,[¥] Luke A. Rochford,[§] Bernard Wenger,[†] Norbert Koch,[¥◊] Henry J. Snaith[*†]

†Department of Physics, Clarendon Laboratory, University of Oxford, Parks Road, Oxford, OX1 3PU, U.K.

¥ Department of Physics, Humboldt Universität zu Berlin, Brook Taylor Straße 6, 12489 Berlin, Germany

§ School of Chemistry, University of Birmingham, University Rd W, Birmingham, B15 2TT, U.K.

◊ Helmholtz-Zentrum für Materialien und Energie GmbH, Albert-Einstein-Straße 15, 12489 Berlin, Germany

The relationship between the chemical composition of lead halide perovskite materials and their crystal and electronic structure is not yet sufficiently understood, despite its fundamental importance. Here, we determine the crystal and electronic structure of cesium lead bromide ($CsPbBr_3$) whilst deliberately varying the cesium content. At sub-stoichiometric concentrations of cesium, there are large variations in the frontier electronic structure of $CsPbBr_3$ with only small variations in Cs content. We observe a critical point after which large variations in the chemical composition of $CsPbBr_3$ result in comparably small changes in valence and conduction band energies. This behavior is starkly different from that of traditional semiconductors, such as InGaAs and GaInP, and demonstrates an impressive energetic tolerance of $CsPbBr_3$ to large changes in its stoichiometry. This observation helps us to understand why a broad range of relatively uncontrolled, simple processing methodologies can deliver highly functional metal halide perovskite thin films.

Introduction

Lead halide based perovskite photovoltaics have emerged in the past years as a technology with great potential to provide affordable renewable energy.[1] These materials offer the simplicity and ease of solution processing whilst possessing direct band gaps and excellent optoelectronic properties combined with high optical absorption coefficients.[2–4] Energy conversion efficiencies of perovskite photovoltaic devices have surpassed 24 %, bringing the technology in line with conventional silicon photovoltaics and making them the fastest developing solar technology to date.[5] Despite the demonstrable potential of perovskite photovoltaics and considerable advances in device efficiencies our understanding of their physicochemical properties remains ambiguous at best. Truly understanding the electronic structure and any structure-property relationships of these materials, is an important step in ensuring ultimate device optimization.

The electronic structure of a perovskite thin film can be heavily influenced by processing conditions; solvent choice, precursors, deposition method, and ambient environment can all alter physical and electronic properties.[6–12] In spite of this there is an impressive degree of tolerance of these materials towards huge differences in processing methods. In conventional semiconductor growth ensuring high purity of the materials and having precise control over their growth is of the utmost importance in producing high performance semiconducting devices.[13–15] Metal halide perovskite materials are unusual in that not only can similarly high performance devices be made following different processing methods but precursor purity appears to not be as critical as with other semiconducting materials.[7,16–19] A vast number of reports detail the influence of such variables on photovoltaic device performance, while studies investigating fundamental chemistry and physics are far less common. Photovoltaic device performance can be improved by fabricating perovskite thin films using precursor solutions in which a stoichiometric excess of one or more of the starting materials precursors exists. [20–23] Despite this, the influence of chemical stoichiometry on the physical and electronic structure of lead halide perovskite materials has not been determined. $CsPbBr_3$ has been utilized in efficient light emitting diode (LED) and photovoltaic devices.[24,25] It is phase stable and experiences significantly less damage, than other lead halide perovskite materials, upon exposure to X-ray and ultraviolet (UV) radiation making it an ideal candidate for a fundamental study of this nature.[26]

Herein, we determine the physical and electronic structure of cesium lead bromide ($CsPbBr_3$) whilst deliberately varying the alkali metal content. Additionally, employing a system containing only one type of halide atom allows us to negate changes to electronic structure, which would be caused by halide segregation. We find that at low concentrations of alkali metal, its overall content has a significant impact on the electronic structure of $CsPbBr_3$ but once a critical point has been reached the frontier energy levels become incredibly invariant with increasing alkali metal content. Overall, our study presents a thorough relationship between the chemical and electronic structure of lead halide perovskite materials.

Experimental Section

Thin film preparation

All films were prepared on ITO coated glass, except those used in the PL measurements which were prepared onto uncoated glass, cleaned using the following solvents: 2 % Hellmanex in deionized water, acetone and isopropanol and treated using

oxygen plasma for 10 minutes. All chemicals were purchased from Sigma Aldrich and used as received and all films were fabricated in a N_2 filled glovebox. Solutions of the appropriate ratios were fabricated using cesium bromide (Alfa Aesar, 99.9 % metals basis) and lead bromide (Alfa Aesar, 98+ %) dissolved in DMSO in the appropriate quantities. Solutions were made up in a N_2 filled glovebox and left to stir overnight prior to film fabrication. Thin films of PEDOT:PSS (Ossila, AI 4083) were spin-coated in dry air onto the clean ITO substrates using 100 µl of solution at 6000 rpm for 45 s. Immediately prior to spin-coating the PEDOT:PSS solution was filtered using a 0.45 µm PTFE filter. The films were then annealed at 150 °C for 10 min and transferred immediately into the glovebox where they were annealed at 150 °C for a further 5 min to ensure minimal water remaining on the surface of the films. The $CsPbBr_3$ films were spin-coated using 50µl of solution onto the cooled PEDOT:PSS/ITO substrates at 4000 rpm for 40 s. An anti-solvent quench of 100 µl of chloroform was dropped onto the substrates after 37 s of the spin-coating process. The films were then annealed at 100 °C for 10 min.

X-ray diffraction (XRD) measurements

X-ray diffraction measurements were carried out using a PANalytical X'Pert Pro MRD diffractometer with monochromatic Cu $K\alpha_1$ radiation.

Ultraviolet-visible spectroscopy measurements

Electronic absorbance spectra were measured in total reflection and transmission mode with a Perkin-Elmer Lambda 1050 UV-vis spectrophotometer equipped with a 100 mm integrating sphere accessory.

Photoluminescence (PL) measurements

Steady state PL measurements were acquired using a Fluorolog Spectrofluorometer (Horiba) and were excited at 370 nm.

Scanning Probe Microscopy (SPM) Measurements

Atomic force microscopy (AFM) measurements were carried out using a Bruker Dimension FastScan system. Measurements were carried out in an ambient environment using Scan Asyst mode and SCANASYST-AIR cantilevers.

Ultraviolet and X-ray Photoemission Spectroscopy (UPS and XPS) measurements

Photoemission experiments were performed using a custom built ultrahigh vacuum (UHV) system (base pressure of 1 x 10^{-10} mbar). Samples were prepared in a N_2 filled glovebox and transferred into the UHV chamber without exposure to atmosphere using a transfer rod which was kept under rough vacuum (1 x 10^{-3} mbar). UPS was carried out using a helium discharge lamp (21.22 eV) and a filter to reduce the photoflux and visible light from the He source. The work function of the samples was determined using the secondary electron cut-off spectra (SECO) recorded with a 10 V bias applied to the sample to overcome the analyzer work function. XPS was carried out using Mg Kα radiation (1253.6 eV) generated from a twin anode X-ray source. All spectra were recorded at normal emission and room temperature using a hemispherical SPECS Phoibos 100 analyzer. The energy resolution of these measurements was 120 meV and 1.2 eV for UPS and XPS respectively.[27]

Inverted photoelectron spectroscopy (IPES) measurements

The IPES measurements were performed in the isochromat mode using a low-energy electron gun with a BaO cathode and a band pass filter of 9.5 eV (SrF2 + NaCl). The energy resolution of IPES was 0.74 eV.[27] The resolution and energy calibration of the PES and IPES were determined by measuring the Fermi edge of a clean Au (111) single crystal. All presented XPS, UPS and IPES spectra given in binding energy (BE) are referenced to the Fermi level, which is at 0 eV.

Results and Discussion

A series of $CsPbBr_3$ thin films with different alkali metal concentrations were fabricated and used to investigate the relationship between their structure and electronic properties. Starting with pure $PbBr_2$ and gradually increasing the alkali metal content, by adding increasing amounts of CsBr in the precursor solution, $CsPbBr_3$ films with a range of stoichiometry were prepared. These compositions are reported in Table 1 and thereafter referred to by the relative molar ratio of CsBr content x to $PbBr_2$ (e.g. x = 0.5). The atomic compositions, as determined through x-ray photoemission experiments are reported in Table S1. Full details of the thin film preparation can be found in the experimental section.

$PbBr_2$	1	1	1	1	1	1	1	1	1	0
CsBr (x)	0	0.01	0.1	0.25	0.5	0.75	1	1.25	1.5	1

Table 1 - Table of relative ratios of precursor materials used to produce thin films of $CsPbBr_3$ with differing alkali metal content.

X-ray diffraction (XRD) measurements were used to investigate the crystal structure of the resulting $CsPbBr_3$ thin films (Figure 1). In all films the majority of Bragg peaks can be attributed to the orthorhombic structure of $CsPbBr_3$ reported by Stoumpos and co-workers.[28] For thin films which have sub-stoichiometric amounts of Cs present $CsPbBr_3$ perovskite is still formed despite a considerable dearth of CsBr relative to $PbBr_2$ in the precursor solution. In addition to diffraction peaks related to $CsPbBr_3$, all films exhibit a peak at 11.8°, which was previously observed in measurements of single crystals of $CsPb_2Br_5$, despite no other peaks corresponding to this structure being measured.[29] At x < 0.5 a peak attributed to $PbBr_2$ (at 22.0°) is observed, but is not present at values of x > 0.5.[30] This suggests that it is only necessary to have more than 50% CsBr, in order to eliminate the crystalline $PbBr_2$ regions being formed in the films.

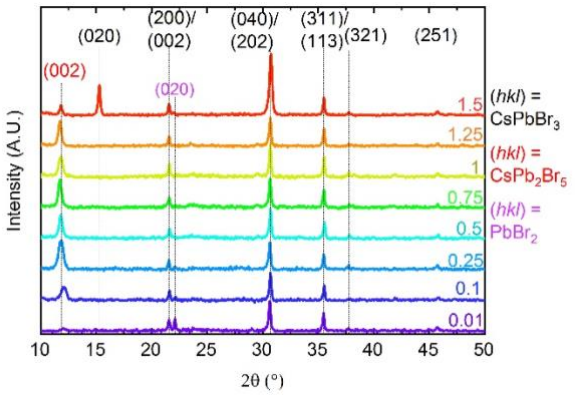

Figure 1 –X-ray diffractograms of $CsPbBr_3$ thin films with varying precursor compositions (x:1), where x is the ratio of CsBr relative to $PbBr_2$. Scans are labelled with the value of x and the color of the assignment text reflects to which crystal structure it corresponds.

Furthermore, the perovskite structure can readily form with 100 times less CsBr than $PbBr_2$. Diffraction patterns for pure CsBr and $PbBr_2$ films and comparison of specific diffractograms with comparison to existing crystal structures can be found in Figures S1 - 4. The morphology of all films was further examined using atomic force microscopy (AFM), as shown in Figure S5. Film thicknesses (also measured using AFM) were found to be between 150 - 200 nm for all compositions. All films were continuous and in those containing the $CsPbBr_3$ perovskite structure the average grain size is between 100 - 200 nm. Predominantly the films appeared uniform except those films where x = 0.01 – 0.75, which contained some significantly larger grains, both in lateral size and height, than the majority of the film. These films contain crystalline $PbBr_2$ (from XRD) suggesting that these larger grains could be $PbBr_2$ crystallites. These samples all exhibit essentially identical X-ray diffraction patterns, confirming that all grains detected by laboratory XRD share the same crystal structure.

The optical absorption and emission of the films was investigated using ultraviolet-visible (UV-vis) and steady-state photoluminescence (PL) spectroscopy, as shown in Figures S6 and S7. The spectra show an excitonic absorption peak for films with x > 0.5 located at 516 nm. For CsBr ratios of 0.01, 0.1 and 0.25 no absorption in the visible range was observed, which was unsurprising since these films appeared colorless to the eye.

All films had emission maxima between 519 - 525 nm, with films corresponding to x ≥ 1 emitting at 525 nm. All other ratios, and x = 1.5, had considerably lower PL intensity and exhibited blue-shifted emission. Full details of the emission and absorption characteristics can be found in Table S2.

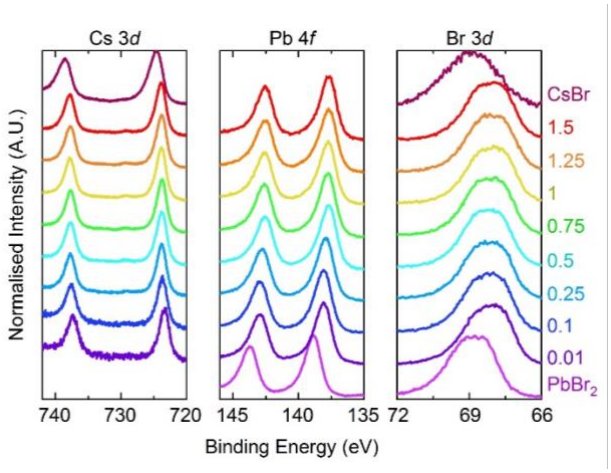

Figure 2 - X-ray photoemission spectra of the Cs 3*d*, Pb 4*f* and Br 3*d* core levels for all compositions of $CsPbBr_3$.

The changes to the chemistry and stoichiometry of the various thin films were examined using X-ray photoemission spectroscopy (XPS). XPS spectra of Cs 3*d*, Pb 4*f* and Br 3*d* core levels are shown in Figure 2 for all $CsPbBr_3$ compositions. Core level peaks are at: ~724 eV (Cs $3d_{5/2}$), ~138 eV (Pb $4f_{7/2}$) and ~68 eV (Br $3d_{5/2}$) for $CsPbBr_3$ with varying x, for pure CsBr at 724.4 eV and 725.3 eV (Cs $3d_{5/2}$) and 68.5 eV (Br $3d_{5/2}$), and for pure $PbBr_2$ at 138.8 eV and 139.8 eV (Pb $4f_{7/2}$) and 68.4 eV (Br $3d_{5/2}$). See Table S3 for exact peak positions. These peak positions agree closely with previous reports of XPS investigations of $CsPbBr_3$, $PbBr_2$ and CsBr respectively.[31,32]

Small shifts in peak position were observed for Pb 4*f* core levels, towards lower binding energy as alkali metal content increases. We note that there are numerous reasons that can contribute to the shifts of core levels in binding energy, and shifts are not necessarily an indicator of a change in the chemical bonding of a material system and/or charge-state of atoms. Indeed for ionic systems (such as metal halide perovskites) the Madelung energy of a system, which arises due to the electrostatic interaction of the ions, must be taken into account to fully understand the core level shifts in binding energy.[33] In particular an increase in the Madelung energy of the system (for example by an increase in the number of ions present) will result in a shift of the peak.[34] This shift is determined by the nature of the ion (cation/anion) and the electrostatic influence it has on the system.[35] In the case of $CsPbBr_3$ an increase in free Cs^+ ions in the system would result in shifting of core level peaks to a higher binding energy. To qualitatively determine if the increase in a given chemical species can be directly correlated to core level shifts, as induced by the change in the Madelung energy of the system Figure S8 shows plots of the difference in binding energy between two of the core levels (e.g. Cs – Pb, 724.4 – 138.8 eV), for each $CsPbBr_3$ composition, and the relative atomic percentage, of a given chemical species, (as determined from fitting of the XPS data). In these plots there is a clear correlation between the change in binding energy difference between the Pb and Cs core levels and increasing Cs content. Lead halide perovskites have a significant ionic character, therefore it is a reasonable assertion that the Madelung energy will play a role in the observed shifts in core levels of elements present in these materials.[36,37] Apparently, the change in Cs^+ ion concentration in the material does impact the Madelung potential experienced by the other elements. However, it is noteworthy that a more accurate quantitative assessment of the influence of the Madelung potential necessitates elaborate theoretical calculations, which is beyond the scope of this work.

The frontier electronic levels of the $CsPbBr_3$ films were studied using ultraviolet photoemission spectroscopy (UPS), as shown in Figure 3. As reported by Endres *et al.* and Zu *et al.*, due to a low density of states (DOS) of the topmost highly dispersive valence band, additionally masked by the proximity of non-dispersive bands, of numerous lead halide perovskites the extrapolation from the leading edge on a linear intensity scale results in an overestimation of the binding energy of the valence band maximum (VBM), and a logarithmic intensity scale provides a more reliable value for the VBM. [19,38] Here, the VBM values were determined using both linear and a logarithmic scale, to enable better comparison to literature using either of the two methods. Table S4 details all values, determined from photoemission experiments, including VBM binding energy values using linear and logarithmic methods, and they are plotted in Fig. 3(e). Whilst there are the expected differences in the values extracted using the two methods, the trends in VBM shifts towards lower binding energy for increasing Cs content are the same. Therefore, the values referred to from this point on will be those determined on a linear scale, however extracted values for the work function and both sets of VBM values can be found in Table S4.

The VBM of $PbBr_2$ was determined to have a binding energy (BE) of 1.83 eV, with respect to the Fermi level, which

increases to 1.95 eV with addition of the lowest concentration of CsBr at x = 0.01. The VBM BE decreases significantly as the CsBr concentration increases (~ 0.1 - 0.4 eV) up to a value of 1.12 eV at x = 0.75, with an overall change of 0.8 eV in the range of x = 0.01 – 0.75. Conversely, thin films with CsBr compositions greater than 0.75 exhibited small differences in VBM BE as the composition was varied, and a value of 0.9 eV was observed at the highest concentration at x = 1.5. For example, despite *double* the content of CsBr in preparation solutions from x = 0.75 to 1.5 there was only a 0.2 eV difference between their VBM values. As discussed previously from XRD measurements (Figure 1), the crystalline $PbBr_2$ domains are only present when $x \leq 0.5$. Given the significant morphological changes for the films up to $x \leq 0.5$, the presence of crystalline $PbBr_2$ in perovskite thin films is expected to have a significant influence on the electronic structure as the spectra measured by UPS are area-averaged and will include contributions from perovskite

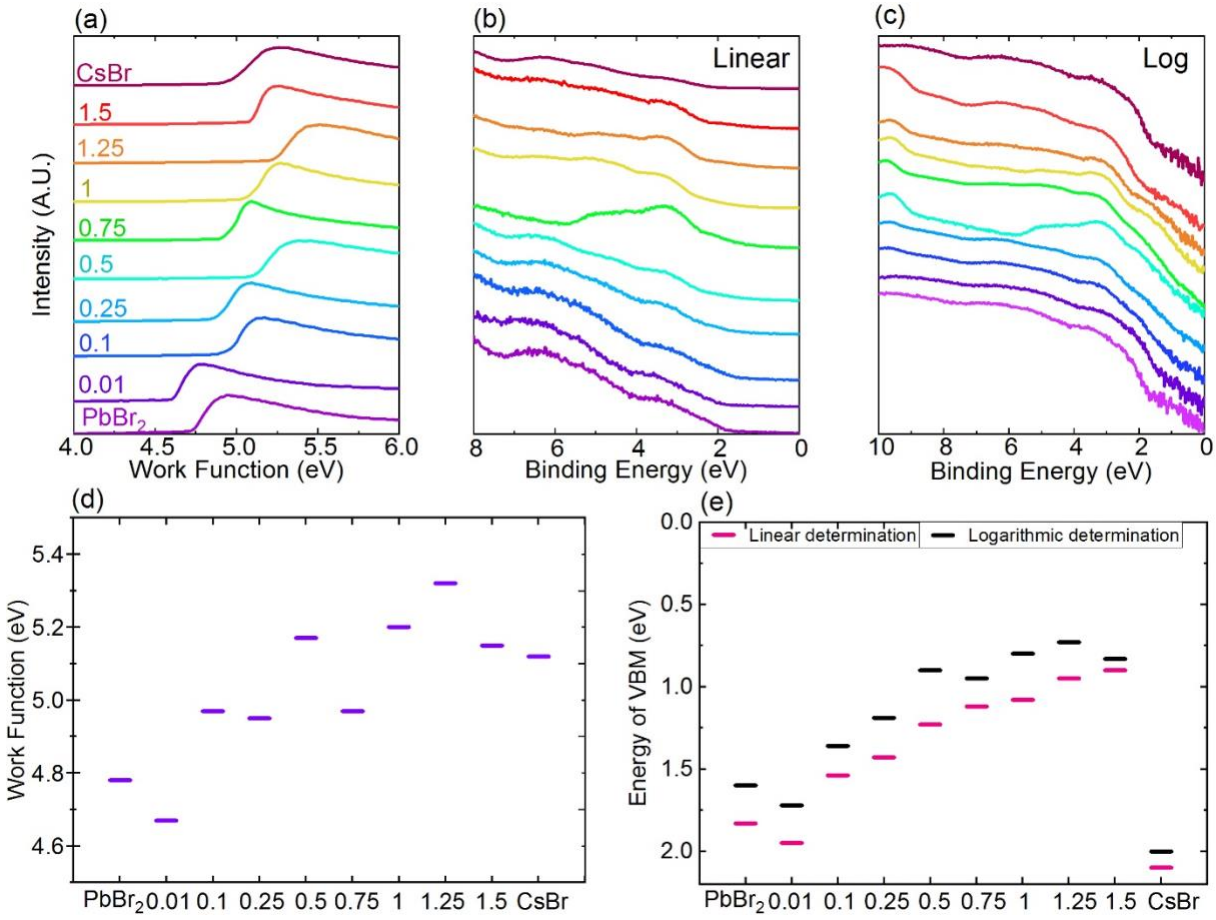

Figure 3 – Ultraviolet photoemission spectra of $CsPbBr_3$ thin films (a) the secondary electron cut-off (SECO), the valence region (b) on a linear intensity scale and (c) on a logarithmic intensity scale, (d) the work function values as determined from the SECO and (e) the valence band maxima (VBM) determined using a linear and logarithmic intensity scale.

and $PbBr_2$ species. This is the most likely reason for significant differences in VBM values between the films with CsBr compositions ≤ 0.5. The most dominant contribution to the electronic structure therefore seems to be from $PbBr_2$, CsBr does not seem to have the same influence on the frontier electronic structure. Films of pure CsBr were found to have a VBM BE of 2.1 eV, which is in good agreement with previous reports.[31]

Across the range of different compositions with $x \geq 0.75$, changes to the VBM position were relatively small. This trend was also observed in the XPS data in Figure 2 where at $x > 0.5$ the binding energy differences change only very slightly, in contrast to significant changes in binding energy differences at $x < 0.5$ with increasing alkali metal content. This would suggest that the electronic structure of $CsPbBr_3$ has a significant tolerance to alkali metal content –once enough alkali metal is present in solution to generate the $CsPbBr_3$ structure the valence and core level binding energy positions remain relatively consistent in energy.

The secondary electron cut-off (SECO) region of the UPS spectra (Figure 3a and 3d) allows the determination of the sample work function. There is an overall trend that an increasing CsBr content results in a higher work function, as summarized in Figure 3d at each sample composition. The work function of the films formed from pure precursors was 4.78 eV for $PbBr_2$ and 5.12 eV for CsBr, in good agreement with previously reported measurements.[31,39] For $CsPbBr_3$ films the highest work function was 5.32 eV, for x = 1.25, and the lowest value was 4.67 eV, for x = 0.01.

To determine the electronic band gap of the $CsPbBr_3$ films the conduction band region was measured using inverse photoemission spectroscopy (IPES) for a selection of alkali metal concentrations, as displayed in Figure 4.

Considering a large experimental broadening in IPES measurements, the conduction band minimum (CBM) was extrapolated using the linear scale plots, as summarized in Table S3.[38,40] The CBM values measured for the various compositions of $CsPbBr_3$ result in electron affinity (EA) values between 3.8 - 4.0 eV, which is in reasonably close agreement with previously reported measurements on $CsPbBr_3$.[19] The difference in CBM values between the compositional ranges is, however, less significant than that observed for the VBM. Reportedly, lead halide perovskites have a small exciton binding energy, < 25 meV for the organic-inorganic lead halide perovskites, which suggests that the measured optical and electronic band gap should be very similar.[4,41] As such we compare the measured optical and electronic band gaps (linear and logarithmically determined) in Figure 4. To estimate the optical bandgap, we fitted the absorption edge using Elliott's model to separate the excitonic peak from the absorption of the continuum of states (see Figure S7 and Supplementary Note 1).[42] The values obtained from UPS and IPES are characteristic of the continuum of states, as confirmed by the absence of excitonic features in these

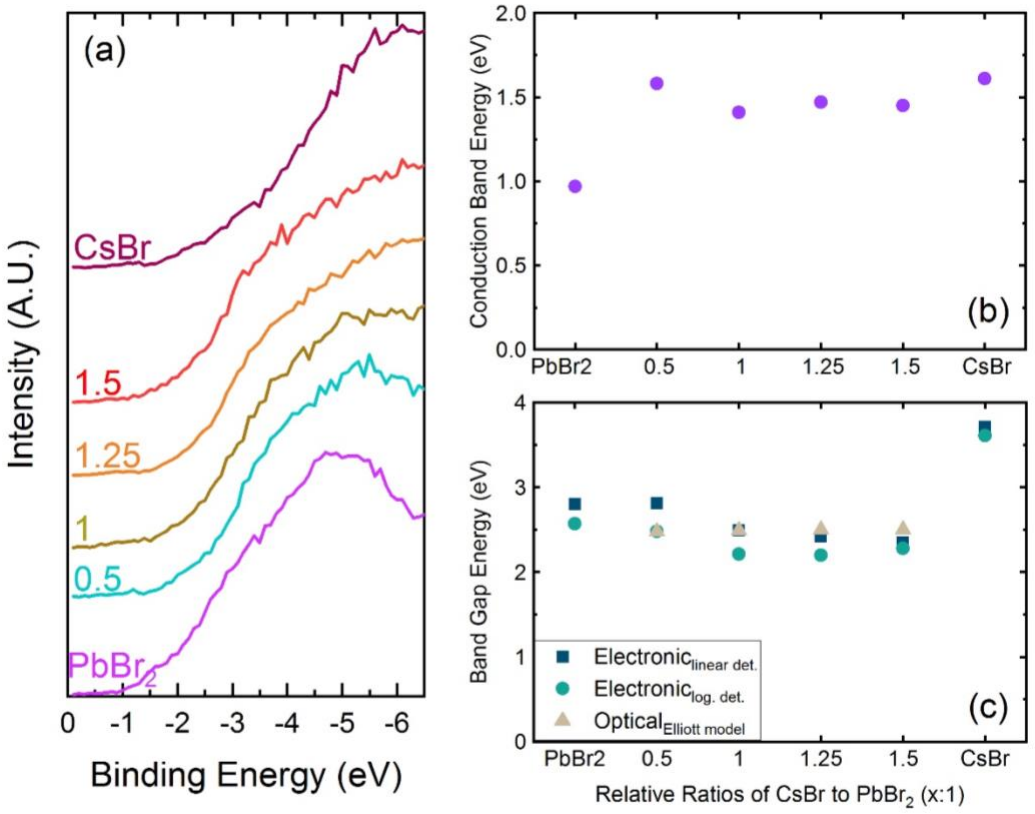

Figure 4 –(a) Inverse photoemission spectra (IPES) of $CsPbBr_3$ thin films of with varying precursor compositions (x:1), where x is the ratio of CsBr relative to $PbBr_2$. (b)The respective conduction band minimum values as determined from the IPES measurements and (c) the electronic and optical band gaps as determined from photoemission and UV-vis absorption spectroscopy. Band $gap_{linear,log} = VBM_{linear,log} - CBM$

spectra. Therefore, we can directly compare the band gaps obtained from the UPS/IPES data to the continuum band edge estimated from the optical absorption.

From $x \geq 0.5$ we have observed a slight narrowing in both the optical and electronic band gap, however, this is caused predominately by changes in the VBM binding energy, and not the

CBM. As with the valence and core levels there is little difference in the measured CBM energies in spite of the significant increase in Cs content between x = 0.5 and x = 1.5. For some compositions the measured electronic band gap appears to be different from the optical band gap. As the onset determination for the CBM proceeds with a considerable error bar for perovskite materials it seems highly likely that the onset determination is responsible for this discrepancy. In the wider context of semiconductor materials this tolerance to alkali metal content is rather unusual. Electronic doping is widely utilized in silicon and III-V semiconductors to tune energy levels, because relatively small amounts of additional chemical species can result in significant changes to energy level positions.13 In this context the small change (ca. 0.2 eV) in VBM values for the films between x = 0.75 to 1.5 (potentially a 100 % increase in Cs content) studied here is rather impressive. In this work, clear evidence has been presented as to the invariance of the electronic structure of lead halide perovskites with significant changes in the composition of the starting solutions and the crystalline thin films. From the XRD measurements, it is apparent that the crystal structure does not vary considerably with changes in stoichiometry and the predominant crystal structure present in the films is the perovskite (ABX_3) polymorph. The XPS measurements show a clear correlation between the ratio of precursors in solution and an excess or deficiency in Cs content in the corresponding thin films (Table S1).Our findings are hence most consistent with the change in composition of the films, indicating a change in the stoichiometry of the perovskite structure rather than being

composed of stoichiometric ABX_3 perovskite domains in a matrix of other polymorphs. However, at present, the underlying origin of this intolerance is not obvious. Since the electronic band structure is controlled by the periodic structure of the lattice, and the atomic orbitals of the constituent elements, we would not expect a significant change to the band structure by simply removing a certain fraction of the atoms, provided the underlying crystal structure remains unchanged. Therefore, in order to understand the origin of our observations, we need to understand why the crystal structure is so tolerant to large deviations from stoichiometry. This is likely to require a combination of experimental and theoretical investigations to resolve, and is beyond the scope of the present work.

Conclusion

Cesium lead bromide thin films with a range of alkali metal concentrations were prepared and the impact of changing the stoichiometry of this material on its structure, morphology, and electronic as well as optical properties was investigated. In compositions with an incredibly low relative ratio of CsBr to $PbBr_2$ (0.01:1) the orthorhombic crystal structure of $CsPbBr_3$ is observed in X-ray diffraction measurements. However, crystalline $PbBr_2$ is found to co-exist in thin films with a relative ratio of CsBr to $PbBr_2$ of up to 0.5:1. Photoemission spectroscopy measurements elucidated a critical alkali metal concentration after which significant increases in Cs content resulted in negligible changes to the valence and conduction band energies. Additionally, we have shown that at low alkali metal concentrations small changes to Cs content can result in large differences to the measured energy levels further emphasizing the importance of alkali metal concentration on the electronic structure of $CsPbBr_3$. These variations in electronic structure occur concomitantly with changes in the crystal structure and morphology of $CsPbBr_3$ thin films. The remarkable performance of lead halide perovskite materials, in spite of the lack of fine control from solution-based fabrication (low purity of precursor materials, lack of morphological control) is truly one of the mysteries of the research field. This impressive tolerance, in terms of energy level positions in the face of such significant changes in chemistry, must be one of the contributing factors to the unprecedented optoelectronic properties of solution-processed lead halide perovskites.

ASSOCIATED CONTENT

Supporting Information.
Morphology measurements, optical data, full energy level details and fitting of photoemission data. This material is available free of charge via the Internet at http://pubs.acs.org.

AUTHOR INFORMATION

Corresponding Author

* Alexandra.ramadan@physics.ox.ac.uk and henry.snaith@physics.ox.ac.uk

Author Contributions

The manuscript was written through contributions of all authors.

ACKNOWLEDGMENT

AJR and HJS acknowledge the Engineering and Physical Sciences Research Council for funding grant numbers EP/M005143/1 and EP/M015254/1. LAR acknowledges the University of Birmingham for funding. BW acknowledges funding from the European Union's Horizon 2020 research and innovation programme under grant agreement No 763977. FSZ acknowledges the Joint Graduate School HyPerCells of the University of Potsdam and the Helmholtz Zentrum Berlin for financial support. MR and NK acknowledge the Helmholtz Energy Alliance "Hybrid Photovoltaics" and the Deutsche Forschungsgemeinschaft (DFG) - Projektnummer 182087777 - SFB 951 for funding.

REFERENCES

(1) Snaith, H. J.; Hacke, P. Enabling Reliability Assessments of Pre-Commercial Perovskite Photovoltaics with Lessons Learned from Industrial Standards. *Nat. Energy* **2018**, *3* (6), 459–465. https://doi.org/10.1038/s41560-018-0174-4.

(2) Li, W.; Wang, Z.; Deschler, F.; Gao, S.; Friend, R. H.; Cheetham, A. K. Chemically Diverse and Multifunctional Hybrid Organic–inorganic Perovskites. *Nat. Rev. Mater.* **2017**, *2* (3), 16099. https://doi.org/10.1038/natrevmats.2016.99.

(3) Wenger, B.; Nayak, P. K.; Wen, X.; Kesava, S. V.; Noel, N. K.; Snaith, H. J. Consolidation of the Optoelectronic Properties of CH3NH3PbBr3 Perovskite Single Crystals. *Nat. Commun.* **2017**, *8* (1), 590. https://doi.org/10.1038/s41467-017-00567-8.

(4) Miyata, A.; Mitioglu, A.; Plochocka, P.; Portugall, O.; Wang, J. T.-W.; Stranks, S. D.; Snaith, H. J.; Nicholas, R. J. Direct Measurement of the Exciton Binding Energy and Effective Masses for Charge Carriers in Organic–inorganic Tri-Halide Perovskites. *Nat. Phys.* **2015**, *11* (7), 582–587. https://doi.org/10.1038/nphys3357.

(5) Kim, H.-S.; Hagfeldt, A.; Park, N.-G. Morphological and Compositional Progress in Halide Perovskite Solar Cells. *Chem. Commun.* **2019**, *55* (9), 1192–1200. https://doi.org/10.1039/C8CC08653B.

(6) Ramadan, A. J.; Rochford, L. A.; Fearn, S.; Snaith, H. J. Processing Solvent-Dependent Electronic and Structural Properties of Cesium Lead Triiodide Thin Films. *J. Phys. Chem. Lett.* **2017**, *8* (17), 4172–4176. https://doi.org/10.1021/acs.jpclett.7b01677.

(7) Ramadan, A. J.; Noel, N. K.; Fearn, S.; Young, N.; Walker, M.; Rochford, L. A.; Snaith, H. J. Unravelling the Improved Electronic and Structural Properties of Methylammonium Lead Iodide Deposited from Acetonitrile. *Chem. Mater.* **2018**, *30* (21), 7737–7743. https://doi.org/10.1021/acs.chemmater.8b03084.

(8) Zu, F.-S.; Amsalem, P.; Salzmann, I.; Wang, R.-B.; Ralaiarisoa, M.; Kowarik, S.; Duhm, S.; Koch, N. Impact of White Light Illumination on the Electronic and Chemical Structures of Mixed Halide and Single Crystal Perovskites. *Adv. Opt. Mater.* **2017**, *5* (9), 1700139. https://doi.org/10.1002/adom.201700139.

(9) Ralaiarisoa, M.; Salzmann, I.; Zu, F.-S.; Koch, N. Effect of Water, Oxygen, and Air Exposure on CH 3 NH 3 PbI 3- X Cl X Perovskite Surface Electronic Properties. *Adv. Electron. Mater.* **2018**, 1800307. https://doi.org/10.1002/aelm.201800307.

(10) Chen, Q.; Zhou, H.; Fang, Y.; Stieg, A. Z.; Song, T.-B.; Wang, H.-H.; Xu, X.; Liu, Y.; Lu, S.; You, J.; et al. The Optoelectronic Role of Chlorine in CH3NH3PbI3(Cl)-Based Perovskite Solar Cells. *Nat. Commun.* **2015**, *6* (1), 7269. https://doi.org/10.1038/ncomms8269.

(11) Burschka, J.; Pellet, N.; Moon, S.-J.; Humphry-Baker, R.; Gao, P.; Nazeeruddin, M. K.; Grätzel, M. Sequential Deposition as a Route to High-Performance Perovskite-Sensitized Solar Cells. *Nature* **2013**, *499* (7458), 316–319. https://doi.org/10.1038/nature12340.

(12) Emara, J.; Schnier, T.; Pourdavoud, N.; Riedl, T.; Meerholz, K.; Olthof, S. Impact of Film Stoichiometry on the Ionization Energy and Electronic Structure of CH 3 NH 3 PbI 3 Perovskites. *Adv. Mater.* **2016**, *28* (3), 553–559. https://doi.org/10.1002/adma.201503406.

(13) Queisser, H. J. Defects in Semiconductors: Some Fatal, Some Vital. *Science (80-.).* **1998**, *281* (5379), 945–950. https://doi.org/10.1126/science.281.5379.945.

(14) Stringfellow, G. B. The Role of Impurities in III/V Semiconductors Grown by Organometallic Vapor Phase Epitaxy. *J. Cryst. Growth* **1986**, *75* (1), 91–100.

https://doi.org/10.1016/0022-0248(86)90229-0.
(15) Horowitz, G. Organic Field-Effect Transistors. *Adv. Mater.* **1998**, *10* (5), 365–377. https://doi.org/10.1002/(SICI)1521-4095(199803)10:5<365::AID-ADMA365>3.0.CO;2-U.
(16) Jung, M.; Ji, S.-G.; Kim, G.; Seok, S. Il. Perovskite Precursor Solution Chemistry: From Fundamentals to Photovoltaic Applications. *Chem. Soc. Rev.* **2019**, *48* (7), 2011–2038. https://doi.org/10.1039/C8CS00656C.
(17) Zhang, Y.; Kim, S.-G.; Lee, D.-K.; Park, N.-G. CH 3 NH 3 PbI 3 and HC(NH 2) 2 PbI 3 Powders Synthesized from Low-Grade PbI 2 : Single Precursor for High-Efficiency Perovskite Solar Cells. *ChemSusChem* **2018**, *11* (11), 1813–1823. https://doi.org/10.1002/cssc.201800610.
(18) Noel, N. K.; Habisreutinger, S. N.; Wenger, B.; Klug, M. T.; Hörantner, M. T.; Johnston, M. B.; Nicholas, R. J.; Moore, D. T.; Snaith, H. J. A Low Viscosity, Low Boiling Point, Clean Solvent System for the Rapid Crystallisation of Highly Specular Perovskite Films. *Energy Environ. Sci.* **2017**, *10* (1), 145–152. https://doi.org/10.1039/C6EE02373H.
(19) Endres, J.; Egger, D. A.; Kulbak, M.; Kerner, R. A.; Zhao, L.; Silver, S. H.; Hodes, G.; Rand, B. P.; Cahen, D.; Kronik, L.; et al. Valence and Conduction Band Densities of States of Metal Halide Perovskites: A Combined Experimental–Theoretical Study. *J. Phys. Chem. Lett.* **2016**, *7* (14), 2722–2729. https://doi.org/10.1021/acs.jpclett.6b00946.
(20) Roldán-Carmona, C.; Gratia, P.; Zimmermann, I.; Grancini, G.; Gao, P.; Graetzel, M.; Nazeeruddin, M. K. High Efficiency Methylammonium Lead Triiodide Perovskite Solar Cells: The Relevance of Non-Stoichiometric Precursors. *Energy Environ. Sci.* **2015**, *8* (12), 3550–3556. https://doi.org/10.1039/C5EE02555A.
(21) Chang, J.; Zhu, H.; Xiao, J.; Isikgor, F. H.; Lin, Z.; Hao, Y.; Zeng, K.; Xu, Q.-H.; Ouyang, J. Enhancing the Planar Heterojunction Perovskite Solar Cell Performance through Tuning the Precursor Ratio. *J. Mater. Chem. A* **2016**, *4* (20), 7943–7949. https://doi.org/10.1039/C6TA00679E.
(22) Meier, T.; Gujar, T. P.; Schönleber, A.; Olthof, S.; Meerholz, K.; van Smaalen, S.; Panzer, F.; Thelakkat, M.; Köhler, A. Impact of Excess PbI 2 on the Structure and the Temperature Dependent Optical Properties of Methylammonium Lead Iodide Perovskites. *J. Mater. Chem. C* **2018**, *6* (28), 7512–7519. https://doi.org/10.1039/C8TC02237B.
(23) Petrus, M. L.; Hu, Y.; Moia, D.; Calado, P.; Leguy, A. M. A.; Barnes, P. R. F.; Docampo, P. The Influence of Water Vapor on the Stability and Processing of Hybrid Perovskite Solar Cells Made from Non-Stoichiometric Precursor Mixtures. *ChemSusChem* **2016**, *9* (18), 2699–2707. https://doi.org/10.1002/cssc.201600999.
(24) Yuan, H.; Zhao, Y.; Duan, J.; Wang, Y.; Yang, X.; Tang, Q. All-Inorganic CsPbBr 3 Perovskite Solar Cell with 10.26% Efficiency by Spectra Engineering. *J. Mater. Chem. A* **2018**, *6* (47), 24324–24329. https://doi.org/10.1039/C8TA08900K.
(25) Kerner, R. A.; Zhao, L.; Xiao, Z.; Rand, B. P. Ultrasmooth Metal Halide Perovskite Thin Films via Sol–gel Processing. *J. Mater. Chem. A* **2016**, *4* (21), 8308–8315. https://doi.org/10.1039/C6TA03092K.
(26) Philippe, B.; Park, B.-W.; Lindblad, R.; Oscarsson, J.; Ahmadi, S.; Johansson, E. M. J.; Rensmo, H. Chemical and Electronic Structure Characterization of Lead Halide Perovskites and Stability Behavior under Different Exposures—A Photoelectron Spectroscopy Investigation. *Chem. Mater.* **2015**, *27* (5), 1720–1731. https://doi.org/10.1021/acs.chemmater.5b00348.
(27) Winkler, S.; Frisch, J.; Schlesinger, R.; Oehzelt, M.; Rieger, R.; Räder, J.; Rabe, J. P.; Müllen, K.; Koch, N. The Impact of Local Work Function Variations on Fermi Level Pinning of Organic Semiconductors. *J. Phys. Chem. C* **2013**, *14*, 130514085014001. https://doi.org/10.1021/jp401919z.
(28) Stoumpos, C. C.; Malliakas, C. D.; Peters, J. A.; Liu, Z.; Sebastian, M.; Im, J.; Chasapis, T. C.; Wibowo, A. C.; Chung, D. Y.; Freeman, A. J.; et al. Crystal Growth of the Perovskite Semiconductor CsPbBr 3 : A New Material for High-Energy Radiation Detection. *Cryst. Growth Des.* **2013**, *13* (7), 2722–2727. https://doi.org/10.1021/cg400645t.
(29) Dursun, I.; De Bastiani, M.; Turedi, B.; Alamer, B.; Shkurenko, A.; Yin, J.; El-Zohry, A. M.; Gereige, I.; AlSaggaf, A.; Mohammed, O. F.; et al. CsPb 2 Br 5 Single Crystals: Synthesis and Characterization. *ChemSusChem* **2017**, *10* (19), 3746–3749. https://doi.org/10.1002/cssc.201701131.
(30) Nieuwenkamp, W.; Bijvoet, J. M. *Zeitschrift Fuer Kristallographie, Kristallgeometrie, Kristallphysik, Kristallchemie (-144, 1977)*; 1932.
(31) Hu, Y.; Wang, Q.; Shi, Y.-L.; Li, M.; Zhang, L.; Wang, Z.-K.; Liao, L.-S. Vacuum-Evaporated All-Inorganic Cesium Lead Bromine Perovskites for High-Performance Light-Emitting Diodes. *J. Mater. Chem. C* **2017**, *5* (32), 8144–8149. https://doi.org/10.1039/C7TC02477K.
(32) Wagner, C. D.; Riggs, W. M.; Davis, L. E.; Moulder, J. F.; Muilenberg, G. E. *Handbook of X-Ray Photoelectron Spectroscopy*; Perkin-Elmer Corporation, Minnesota, 1979.
(33) Bagus, P. S.; Ilton, E. S.; Nelin, C. J. The Interpretation of XPS Spectra: Insights into Materials Properties. *Surf. Sci. Rep.* **2013**, *68* (2), 273–304. https://doi.org/10.1016/j.surfrep.2013.03.001.
(34) Watson, R. E.; Davenport, J. W.; Perlman, M. L.; Sham, T. K. Madelung Effects at Crystal Surfaces: Implications for Photoemission. *Phys. Rev. B* **1981**, *24* (4), 1791–1797. https://doi.org/10.1103/PhysRevB.24.1791.
(35) Taucher, T. C.; Hehn, I.; Hofmann, O. T.; Zharnikov, M.; Zojer, E. Understanding Chemical versus Electrostatic Shifts in X-Ray Photoelectron Spectra of Organic Self-Assembled Monolayers. *J. Phys. Chem. C* **2016**, *120* (6), 3428–3437. https://doi.org/10.1021/acs.jpcc.5b12387.
(36) Glasser, L. Solid-State Energetics and Electrostatics: Madelung Constants and Madelung Energies. *Inorg. Chem.* **2012**, *51* (4), 2420–2424. https://doi.org/10.1021/ic2023852.
(37) Kerner, R. A.; Rand, B. P. Ionic–Electronic Ambipolar Transport in Metal Halide Perovskites: Can Electronic Conductivity Limit Ionic Diffusion? *J. Phys. Chem. Lett.* **2018**, *9* (1), 132–137. https://doi.org/10.1021/acs.jpclett.7b02401.
(38) Zu, F.; Amsalem, P.; Egger, D. A.; Wang, R.; Wolff, C. M.; Fang, H.; Loi, M. A.; Neher, D.; Kronik, L.; Duhm, S.; et al. Constructing the Electronic Structure of CH 3 NH 3 PbI 3 and CH 3 NH 3 PbBr 3 Perovskite Thin Films from Single-Crystal Band Structure Measurements. *J. Phys. Chem. Lett.* **2019**, *10* (3), 601–609. https://doi.org/10.1021/acs.jpclett.8b03728.
(39) Heidrich, K.; Schäfer, W.; Schreiber, M.; Söchtig, J.; Trendel, G.; Treusch, J.; Grandke, T.; Stolz, H. J. Electronic Structure, Photoemission Spectra, and Vacuum-Ultraviolet Optical Spectra of CsPbCl3 and CsPbBr3. *Phys. Rev. B* **1981**, *24* (10), 5642–5649. https://doi.org/10.1103/PhysRevB.24.5642.
(40) Park, S.; Mutz, N.; Schultz, T.; Blumstengel, S.; Han, A.; Aljarb, A.; Li, L.-J.; List-Kratochvil, E. J. W.; Amsalem, P.; Koch, N. Direct Determination of Monolayer MoS 2 and WSe 2 Exciton Binding Energies on Insulating and Metallic Substrates. *2D Mater.* **2018**, *5* (2), 25003. https://doi.org/10.1088/2053-1583/aaa4ca.
(41) Galkowski, K.; Mitioglu, A.; Miyata, A.; Plochocka, P.; Portugall, O.; Eperon, G. E.; Wang, J. T.-W.; Stergiopoulos, T.; Stranks, S. D.; Snaith, H. J.; et al. Determination of the Exciton Binding Energy and Effective Masses for Methylammonium and Formamidinium Lead Tri-Halide Perovskite Semiconductors. *Energy Environ. Sci.* **2016**, *9* (3), 962–970. https://doi.org/10.1039/C5EE03435C.
(42) Elliott, R. J. Intensity of Optical Absorption by Excitons. *Phys. Rev.* **1957**, *108* (6), 1384–1389. https://doi.org/10.1103/PhysRev.108.1384.

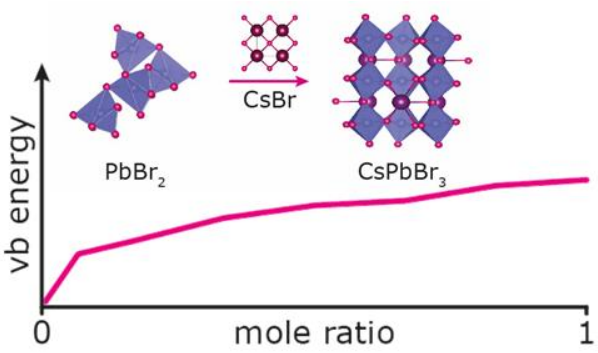
PbBr2
CsBr
CsPbBr3
vb energy
0
mole ratio
1